IEEE Access
Multidisciplinary | Rapid Review | Open Access Journal

Received 5 June 2025, accepted 23 July 2025, date of publication 30 July 2025, date of current version 7 August 2025.

Digital Object Identifier 10.1109/ACCESS.2025.3593937

APPLIED RESEARCH

Assessing Head Injury of Civilian UAV Safety Systems: A Test Apparatus and Spherical Shell Example

ERIC J. HETTEL[1], HOSSEIN ESLAMIAT[1], MOHAMMED ALEEMUDDIN[1], AND MOHSEN FARAJIJALAL[2]

[1]School of Mechanical, Aerospace, and Materials Engineering, Southern Illinois University, Carbondale, IL 62901, USA
[2]Department of Mechanical Engineering, University of California at Merced, Merced, CA 95343, USA

Corresponding author: Hossein Eslamiat (hossein.eslamiat@siu.edu)

This work was supported in part by the School of Mechanical, Aerospace, and Materials Engineering at Southern Illinois University, Carbondale, USA.

ABSTRACT In recent years, flying vehicles have become an innovative way to transfer parcels efficiently over a short distance. Existing airspace regulations are slow to adapt to the anticipated rise in aircraft traffic resulting from this development. This is because the increase in unmanned aerial vehicles (UAVs) comes with an increased risk of personal injuries from faulty drones carrying a payload. Many national regulatory agencies, such as the FAA, rely on the Abbreviated Injury Scale (AIS) to determine the weight threshold of a UAV by evaluating the impact energy and correlating it to the severity of a potential injury. This research paper presents a test apparatus to investigate the effect of different safety systems on AIS.As an example, a passive safety system in the form of a geodesic shell is used to investigate the change in impact acceleration and therefore, the head injury sustained. The spherical shell is designed as a geodesic sphere. Its struts are carbon fiber reinforced polymer (CFRP) rods and connectors made from a flexible filament, TPU-95A. The apparatus enables droppings of the geodesic shell from a height of 4.48 meters,varying the payload weight in two weight classes between 2.5 lb to 5 lb attached to the drone. The impact acceleration is recorded, and the impact velocity is calculated using slow-motion video. The Head Injury Criterion (HIC) scale and the Abbreviated Injury Scale (AIS) are used to measure the predicted head injury level. The test apparatus designed establishes a standard of testing for other safety systems, in addition to geodesic shells like airbags, to be tested for their efficacy in reducing the head injury level sustained.

INDEX TERMS Aerospace safety, collision tolerance, drones, injuries, spherical shell, UAV crash testing.

I. INTRODUCTION

The use of drones for commercial and recreational purposes has increased dramatically in the past decade. Civilian multirotor drones represent a modern and rapidly evolving technology with expanding applications across diverse fields, including delivery service [1], precision agriculture [2], [3], [4], mining [5], disaster management [6], aerial light shows [7], and transportation monitoring [8]. Many companies are now exploring the use of drones for last-mile deliveries. Companies like Google, Amazon, and UPS have launched drone fleets that are being tested for use in last-mile deliveries. Wing, which is a subsidiary of Alphabet, the holding company for Google and Waymo, is using a hybrid fixed-wing unmanned aerial vehicle (UAV) to deliver packages up to 7 pounds. UPS Flight Forward is a subsidiary of UPS that focuses on last-mile pharmaceutical product delivery. They have partnered with CVS to use drones to deliver prescriptions to residents of The Villages in Florida [9]. This market of drone package delivery, once fully launched and regulated, is expected to grow to a 58.4 billion dollar/year market [10]. The FAA released an Unmanned Aircraft Systems (UAS) Beyond Visual Line-of-Sight (BVLOS) Aviation Rulemaking Committee (ARC) final report in March 2022 that recommends an overhaul of existing regulations and the creation of new regulations to

The associate editor coordinating the review of this manuscript and approving it for publication was Agustin Leobardo Herrera-May.

enable industry growth. One recommendation made by the Committee is not to limit small UAS (weighing less than 55lbs or 25,000 ft-lb of KE) from conducting BVLOS operations. Furthermore, the committee suggests that different means of compliance for unmanned aircraft (UA) with less than 500 ft-lb of kinetic energy are different than those with 25,000 ft-lb of kinetic energy due to the decreased risk posed by UAVs of lower kinetic energy thresholds [11]. One proposition is that if a manufacturer can prove that their UA cannot cause damage greater than a three on the AIS, it will facilitate an expedited BVLOS waiver or an Airworthiness certificate for the commercial drone. AIS3 correlates to injuries that are deemed Minor to Serious and not Severe, Critical, or Unrevivable [12]. Unintended collisions are a recognized risk when operating unmanned aircraft, prompting extensive efforts to develop collision-resistant safety mechanisms. While advanced sensors and computational techniques are commonly utilized for collision avoidance, physical solutions like Rotor Cages serve as a reliable safeguard in scenarios where these methods may be insufficient. These protective devices enhance safety during operations in overpopulated areas and within confined spaces. For outdoor applications such as bridge inspections, large pipeline assessments, and mining operations, the presence of obstacles makes Rotor Cages essential. By incorporating such protective structures, drones can navigate complex and dynamic environments safely, reducing reliance on sophisticated collision avoidance systems [13]. If a rotor cage can be proven to mitigate injury levels to a nonfatal degree, it can be employed as an effective safety device for use in operations over people and BVLOS missions.

This study presents the development of a test apparatus and a geodesic drone shell, fabricated using 3D printing and assembled for experimental evaluation. The structure is subjected to drop tests from a height of 4.48 meters, during which impact energy and acceleration are recorded. The associated risk of head injury is assessed using the AIS based on established criteria. Two payload categories, 2.5 lb and 5 lb, are tested. The 4.48-meter drop height can simulate conditions under which conventional safety mechanisms, such as parachute systems, typically requiring a minimum deployment altitude of 20 meters, would not be viable. The custom-built drop test apparatus is employed to facilitate these experiments.

A. LITERATURE REVIEW

There have been many proposed devices to enhance the resilience of UAVs or mitigate injuries sustained in a crash. Some research attempts have been made in collision avoidance software with varying degrees of success. However, collision avoidance software relies on a continuous power supply that is not always guaranteed during an emergency in a UAV flight. Additionally, passive safety features like parachutes or rotor cages can reduce impact energy or injuries without relying on controlling the attitude of the UAV or a continuous power supply. On the other hand, the application of artificial intelligence algorithms in predictive modeling [14] can support the implementation of preventive measures to avert potential collisions, thereby enhancing safety, particularly in UAVs [15], [16].

Recent research has also explored methods to optimize UAV trajectories with a focus on minimizing energy consumption, which indirectly contributes to operational safety by reducing high-energy maneuvers. For instance, Bianchi et al. [17] proposed a hierarchical real-time control framework for UAVs that leverages rule-based reference generation derived from optimal control solutions. Their method identifies common patterns in energy-optimal trajectories and mission durations, enabling the extraction of simple, low-cost rules that closely approximate optimal energy performance while remaining computationally efficient for on-board implementation. Such control strategies are particularly useful when UAVs operate in energy-constrained scenarios or are expected to carry additional safety hardware, such as geodesic shells.

In another research, Mubdir and Prempain [18] introduced an energy-efficient nonlinear model predictive control (NMPC) framework that optimizes quadrotor trajectories while accounting for the UAV's dynamics, constraints, and energy consumption. Their approach leverages online optimization to ensure real-time adaptability and performance, resulting in smoother and safer flight profiles. Integrating such control strategies with passive safety mechanisms, like geodesic shells, can significantly reduce the likelihood and severity of injuries in crash scenarios by both mitigating impact energy and improving control stability during unexpected disturbances.

Al-Madani et al. [19] developed a parachute recovery system with a 1.45-meter diameter to regulate the freefall descent of a 2-kilogram drone, ensuring that its descent speed did not exceed 5 meters per second. The system was designed to deploy the parachute only when an accelerometer detected a predefined threshold acceleration within a specified time interval. Experimental flight tests indicated that a minimum altitude of approximately 20 meters was required for the parachute to fully deploy. Consequently, the risk of serious injury remains unmitigated for flights conducted below this altitude, even with the parachute recovery system in place.

In [20], researchers developed a multipurpose low-altitude drone equipped with a parachute recovery system. The drone had an approximate weight of 4–5 kilograms. The parachute canopy was designed with a diameter of 1.4 meters, accompanied by a pilot chute measuring 0.18 meters. The target descent rate was set at 4.6 meters per second. To ensure effective deployment, researchers determined that the parachute should be deployed at a minimum altitude of 20 meters above ground level (AGL).

Piancastelli et al. [21] analyzed the design considerations for a remote parachute system capable of handling a maximum payload of 80 kilograms. The minimum deployment height was assessed based on the altitude loss required to achieve the desired vertical velocity of 2 meters per

TABLE 1. Comparison of parachute safety systems with related studies.

Reference	Type of Safety Device	Weight of Drone (kg)	Descent Rate (m/s)	Minimum Height (m)
Al-Madani, Basem et al., 2018 [19]	Parachute	2	5	20
Indurkar, I. et al., 2021 [20]	Parachute	4 - 5	4.6	20
Piancastelli, Luca et al., 2018 [21]	Parachute	10	2	25

second for parachute deployment. The study evaluated the minimum deployment heights for UAVs ranging from 10 to 150 kilograms. The findings indicated that for a 150-kilogram UAV, the parachute system must be deployed at an altitude of at least 53 meters, while a 10-kilogram UAV requires a minimum deployment height of 25 meters. These results, along with other research, highlight the necessity of a safety device capable of effective operation at low altitudes. Table 1 presents a comparative analysis of parachute safety systems from various studies.

B. SAFETY SHELLS

Spherical frames offer comprehensive protection, in contrast to rotor guards, which provide coverage in only a single plane. Edgerton et al. [22] developed an innovative cage featuring three orthogonal rings, which was 3D-printed and subjected to stress analysis using finite element analysis (FEA). The finalized design of the structured cage is illustrated in Figure 1a. The simulated testing involved applying a force at the most critical point of the structure, specifically at a single joint of the orthogonal rings. A 150N force was applied to the structure, and the resulting stress and displacement were analyzed. The FEA results revealed that the stress values exceeded the material's stress-strain limits, suggesting the potential for cracking or failure under low-impact collisions.

Dave et al. [23] proposed a design for a forestry monitoring UAV with a collision-tolerant spherical frame for 360° collision protection. The structural strength of various protective cages was validated by performing stress analysis in SolidWorks. The simulations found that a truncated icosahedron shell would be the optimum spherical frame. The spherical frame was made from Thermoplastic Polyurethane (TPU) 3D-printed connectors and Carbon-Fiber Reinforced Polymer (CFRP) rods, along with a TPU printed coaxial system for attaching to the drone and rotating about the drone's pitch axis. The drone was then experimentally tested in various indoor spaces using a Q450 frame UAV. The experimental results were found to be viable during indoor test flights, as shown in Figure 1b. However, no drop test simulations were performed, and no stress analysis results were shown.

Mizutani et al. [24] developed a passive rotating spherical shell (PRSS) designed for attachment to a UAV for operations in confined spaces. The PRSS is integrated with the UAV via a 3-degree-of-freedom (D.O.F) gimbal mechanism, allowing the UAV to maintain flight stability during collisions. Several design parameters were evaluated for the spherical shell, with the following identified as the most critical during the design phase:

1) Sphericity of the spherical shell,
2) Diameter of the spherical shell,
3) Payloads,
4) Strength of the spherical shell, and
5) Space for mounting sensors and a UAV.

The final design selected was that of a geodesic sphere with triangular faces, with the number of divisions represented by nV. The number of divisions from 1V to 4V was considered based on the rollover angle of the spherical cage on an inclined plane. The 2V division was selected based on structural strength and risk of rollover during bridge inspections. The geodesic spherical shell was made out of carbon-fiber reinforced polymer (CFRP) spherical rods and 3D-printed connectors of ABS plastic, as shown in Figure 1c. A drop test was performed to determine the structural strength of the shell. With an assumed maximum flight speed of 2.5m/s, the height needed is 0.4m to achieve the maximum flight speed. At a height of 0.4m with a dummy load of 2kg, which is equivalent to the maximum weight of the PRSS UAV, 10 drop tests were performed with no apparent visible damage. However, no experiments were performed to determine the maximum impact load before structural failure.

Additionally, de Azambuja et al. [25] designed a sub-250g collision-resilient quadcopter featuring a semi-rigid structure in the form of a rectangular prism, as illustrated in Figure 1d. The drone's onboard electronics are mounted on a rigid internal frame, 3D-printed using acrylonitrile butadiene styrene (ABS). This internal frame is connected to the exoskeleton through flexible joints made of thermoplastic polyurethane (TPU-95A), providing effective impact damping.

Zha et al. [26] proposed a model-based design method for selecting tensile components in tensegrity aerial vehicles, using dynamic simulations to predict collision stresses. They also developed an autonomous reorientation controller that enables the drone to self-right after impact. This combination of impact resilience and self-reorientation makes the design well-suited for cluttered environments, as demonstrated in forest testing. An example icosahedron-based design is shown in Figure 1e.

In a separate study, De Petris et al. [27] presented a collision-tolerant aerial robot engineered for autonomous subterranean exploration. Designed specifically for underground environments, the system emphasizes structural resilience, reliable autonomy with accurate localization and mapping, and advanced path planning for navigating confined and obstacle-rich spaces. A prototype of the drone and its structural frame is shown in Figure 1f.

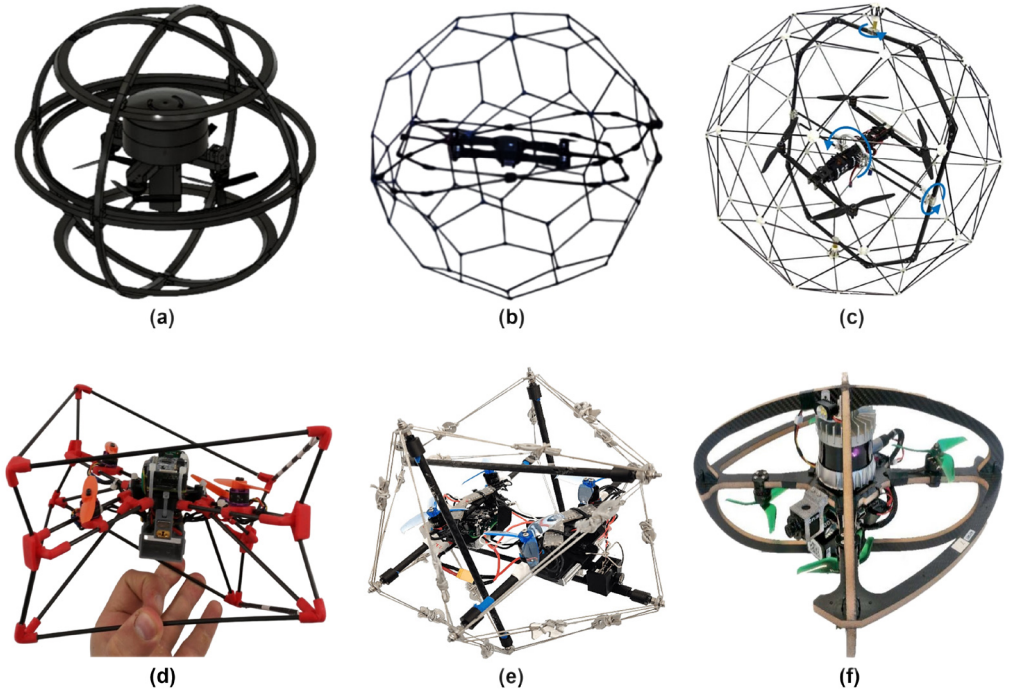

FIGURE 1. Examples of collision-tolerant drone structures explored in various studies: (a) A 3D-printed cage with three orthogonal rings was developed and evaluated using FEA [22]; (b) A forestry monitoring UAV equipped with a collision-tolerant spherical frame providing 360° impact protection [23]; (c) A passive rotating spherical shell (PRSS) engineered for integration with UAVs to enable safe operation in confined environments [24]; (d) A sub-250g collision-resilient quadcopter designed with a semi-rigid rectangular prism structure [25]; (e) An icosahedron tensegrity aerial vehicle developed using the proposed model-based design methodology [26]; (f) A collision-tolerant aerial robot designed for robust autonomous exploration in subterranean environments [27].

C. INJURY SCALE AND UAV FREEFALL

Some research has been done to determine the weight threshold for drones to keep injuries at a level that is nonfatal. Koh et al. [28] studied the weight thresholds of drones based on levels of injury to the human head when the drone is dropped from a specific height. Two well-established indicators of head injuries due to impact are used to measure the level of injury, known as the Head Injury Criterion (HIC) and the Abbreviated Injury Scale (AIS). Examples of head injury classification using AIS can be seen in Table 2.

TABLE 2. AIS and head injury [28].

Injury Level	AIS Code	Head Injury Example
Minor	1	Headache
Moderate	2	Unconcious less than 1h; Linear Fracture
Serious	3	Unconcious 1-6h; Depressed Fracture
Severe	4	Unconcious 6-24h; Open Fracture
Critical	5	Unconcious >24h; Large Hematoma
Unsurvivable	6	Unsurvivable fracture

The purpose of the study was to determine the weight threshold to keep injuries at an AIS level of 3, which represents serious injury and a probability of death between 8 and 10 percent. Small UAVs of varying masses (305g, 405g, 565g, 700g, and 820g) and large UAVs (1.4kg, 2.1kg, 2.6kg, 3.1kg, 5.1kg, 7kg, 9kg, and 11kg) were dropped from varying heights from 10ft to 200ft. Results were both simulated using FEM analysis and experimentally measured. The results from the study suggested that to keep injuries at AIS3, the maximum threshold of impact energy is 95J.

The experiment was performed using a Hybrid III crash test dummy head attached to a 3-spring vertical platform to simulate the vertical spring constant of the human neck. Inside the dummy head were three one-axis accelerometers to detect acceleration in the X, Y, and Z directions. The mobile hanging platform used to drop the drone was made of one 90-degree bent aluminum bar, an electromagnet, and a supporting plate. Guiding wires were placed on 2 UAV arms to ensure the same orientation of the drone during free fall. Weights were then epoxied and attached to the drone to simulate different weight classes. When the experiment was performed, power would be cut to the electromagnet, and the drone would start freefall. The study also focused on identifying limits to weight based on keeping injuries to a maximum level of AIS3. This part of the study determined the maximum weight allowable from a certain height to sustain AIS3 injuries. It was found at the maximum height of 200ft, UAV weight would need to be limited to 0.256kg or 0.56lbs. Table 3 shows the results for all measured heights.

Furthermore, in future works that can be extended from the study, the authors indicate that passive safety features like energy-absorbing materials or parachutes that could increase

TABLE 3. Maximum operating height of UAVs with the respective weight based on ASI3 [28].

Height (in m)	Height (in ft)	UAV Max Weight (kg)
7.62	25	1.298
15.24	50	0.668
22.86	75	0.471
30.45	100	0.978
38.1	125	0.325
45.72	150	0.293
53.34	175	0.271
60.96	200	0.256

the weight threshold while maintaining AIS3 are aspects that deserve further study.

In another study, Zhang et al. [29] conducted an experiment to simulate and experimentally perform a collision with a drone using large landing skis. The target falling speed for the UAV was 10m/s, resulting in a drop height of 5102mm or 16.75ft. The UAV used for the experiments weighed 20.50kg, with a maximum load of 100kg. The experimental results showed a peak impact load of 9.88kN, while the simulated results predicted a 10.57kN peak impact load, an error of 6.53%. Based on the work in [30], AIS level 3 corresponds to an impact load between 5.5kN and 11kN. This suggests that the work in [29] is validated by the work in [30] as it suggests that heavier drones flown at around 20 feet or below would not result in greater than AIS3 level injuries.

II. METHODOLOGY

Several prominent designs are effective in mitigating impact energy, including the geodesic sphere, the truncated icosahedron, and the orthogonal crossbar design. Based on the literature review, the most promising design that is viable for reducing impact energy is the geodesic sphere. From the work done in [24], the design has been experimentally proven to withstand drop tests of a 2kg weight from a height of 0.4 meters. The sphere was designed to fit a QAV 250 quadcopter frame. An FEA analysis was performed on the design, evaluating the maximum stress experienced using a nominal force on the structure. The designed structure was then fabricated using an FDM 3D printer for the connectors and hand-assembled to make the final design.

As shown in the thesis of Eric Hettel [31], the selected spherical design is a geodesic sphere with 2V divisions. This division level was chosen to maintain the spherical shape while minimizing the number of connections, thereby reducing the overall weight of the structure. Figure 2(a) illustrates the 2V division geodesic dome design. The design incorporates two distinct strut lengths and connector types. To accommodate a QAV 250 frame, the inner diameter of the dome is set at 550 mm, ensuring a 25 mm clearance from each rotor blade. Consequently, the A struts measure 137 mm, while the B struts are 155 mm in length. The A struts are positioned at an angle of 15.86°, whereas the B struts are angled at 18°.

A. 3D PRINTING AND MATERIALS

The connectors for the geodesic shell were manufactured using the Raise3D Pro3 Plus FDM printer. This high-performance printer supports a wide range of filaments with extrusion temperatures of up to 300°C, including PLA, ABS, HIPS, PC, TPU, TPE, PETG, ASA, PP, PVA, Nylon, and fiber-reinforced materials such as glass fiber and carbon fiber composites. The TPU was selected for this application due to its high flexibility and elastic behavior. Its rubber-like characteristics make it particularly effective for impact absorption. The specific material used was TPU-95A filament, manufactured by Raise3D. This filament was utilized in the fabrication process and subsequently subjected to mechanical testing, with the results summarized in Table 4. Based on the evaluated properties, TPU-95A was identified as an optimal material for dissipating impact energy, enabling the connectors to deform appropriately under load prior to failure.

TABLE 4. Material properties of selected filaments.

Property	Value
Density (g/cm^3)	1.2 ± 0.2
Young's Modulus (MPa)	9.5 ± 0.4
Tensile Strength (MPa)	29.3 ± 2.8
Elongation at Break (%)	330 ± 15

To ensure consistency, both the drone connectors and shell connectors were printed using the same settings. Table 5 details the printing parameters used for fabricating the connectors.

TABLE 5. Settings for drone and shell connectors [32].

Property	Value
Infill (%)	70
Infill Pattern	Honeycomb
Extruder Temperature (^{o}C)	220
Bed Temperature (^{o}C)	55
Layer Height (mm)	0.1

Figures 2(b) and 2(b) present the designed and fabricated geodesic shell connectors, respectively. The indented line at the top of the connectors aligns with the yellow tubes in the CAD model, which provide support for the A struts, while the remaining tubes support the B struts. The connectors securing the drone to the shell were specifically designed to fit the QAV 250 frame without interfering with the 5-inch rotor blades. These connectors also provided stability in both the horizontal and vertical directions to withstand impacts to the bottom of the drone. Each drone connector was fitted with a single CFRP rod, as shown in Figure 2(d). Additionally, the bottom connector that was mounted on the QAV250 frame can be seen in Figure 2(e).

In the final stage of the design process, the arrangement of the struts is depicted in Figure 2(f). The geodesic dome structure was constructed using CFRP rods with a diameter

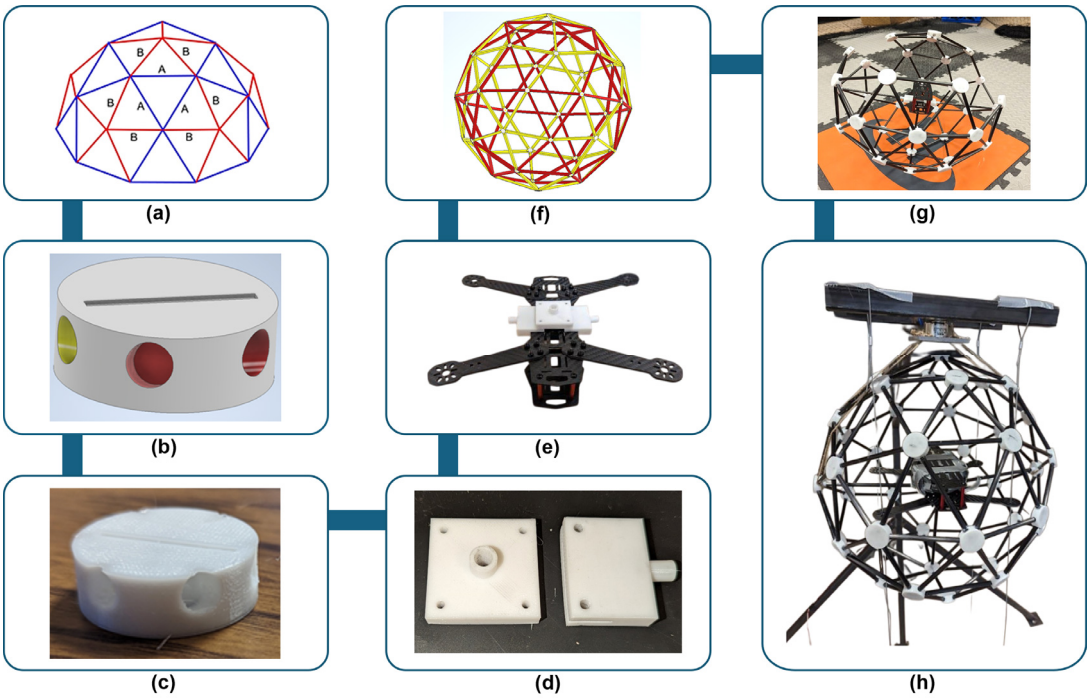

FIGURE 2. Design and fabrication process of the spherical shell: (a) 2V geodesic dome design; (b) Spherical shell connector design in AutoCAD; (c) 3D-printed connector; (d) Connector interface between drone and frame; (e) Bottom connector mounted on the QAV250 frame; (f) Assembled geodesic sphere modeled in AutoCAD; (g) Assembling the geodesic shell parts; (h) Fully assembled geodesic shell with drone prior to drop testing.

of 6 mm. Figure 2(g) illustrates the assembly of the geodesic shell components, including the connectors and rods. The fully assembled geodesic shell undergoing a drop test is shown in Figure 2(h).

B. DROP TEST PLATFORM

A drop test platform was designed, constructed, and successfully tested to measure the impact force and energy of a UAV experimentally. The platform incorporated steel guide wires to maintain a consistent drone orientation across repeated tests while minimizing any influence on its freefall velocity. Additionally, a slow-motion video recording was utilized to capture the failure mechanism of the UAV and accurately measure its impact velocity. The platform also facilitated the recording of impact acceleration and was equipped with compression springs to simulate the spring constant of the human neck.

The drop test platform is composed of two subsections: the Upper Platform and the Lower Platform. The Upper Platform features a mobile hanging structure equipped with an electromagnet designed to release the UAV without any mechanical connection. This structure was constructed using 1-inch square bars of hot-rolled steel, which were welded together for durability and stability. A bracket securely holds the steel guide wires at the end of the Upper Platform, ensuring alignment concentric with the drone's rotors. Guide wires are being used to achieve an almost entirely vertical impact, with accelerations along the x and y axes assumed to be negligible. The Upper Platform is positioned 4.48 meters above the Lower Platform. Figure 3 provides a detailed view of the Upper Platform and its components.

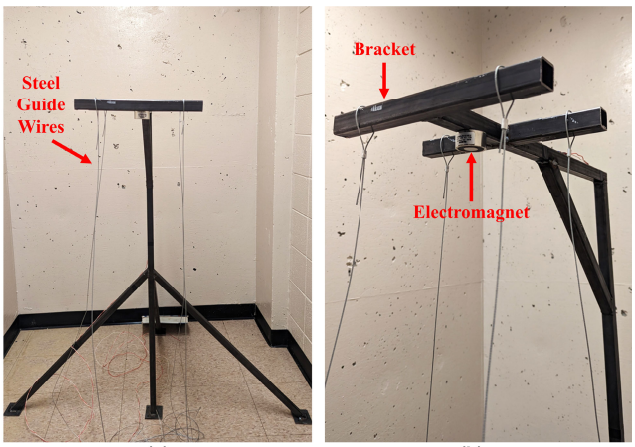

FIGURE 3. Comprehensive view of the constructed upper platform with labeled components: (a) Front view of the platform; (b) Placement of brackets and electromagnet.

The Lower Platform comprises two flat steel plates with three interposed compression springs designed to simulate the spring constant of the human neck. The selection of three compression springs was based on their availability from suppliers and their ability to approximate the neck's spring constant closely. Additionally, this configuration was chosen to align with the design utilized by Koh et al. [28], facilitating an accurate comparison.

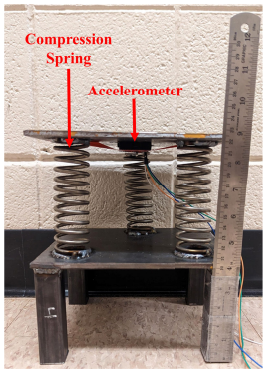

FIGURE 4. A full view of the lower platform.

According to Ciunel et al. [33], the spring constant of the human neck is approximately 114.2 lbf/in. The compression springs used in this study have a spring constant of 35.47 lbf/in and are arranged in parallel. The resulting total spring constant of the assembly is calculated to be 106.41 lbf/in, closely approximating the spring force observed in the average human neck. Given the available options from suppliers, this value represents the closest feasible match to the target spring constant of 114.2 lbf/in. An accelerometer is mounted on the underside of the top plate to capture impact acceleration. The selected sensor for the Lower Platform is a GY-521 MPU6050 3-axis accelerometer, which interfaces with Arduino software for data acquisition. Additionally, a ruler is positioned on the front side of the Lower Drop Test Platform to measure displacement for impact velocity calculations. Figure 4 presents a detailed view of the Lower Platform.

The drop test platform was installed in Alumni Hall at Southern Illinois University, with the Upper Platform positioned 4.48 meters above the Lower Platform. The design of the apparatus allows for adjustable drop heights, providing flexibility in testing conditions. Additionally, the incorporation of counterweights on the Upper Platform enables the accommodation of various payload weights. The complete assembly during a drop test is illustrated in Figure 5.

C. EXPERIMENTAL SETUP AND TESTING VARIABLES

The experiments were conducted for two classes of drone weights, with a fixed initial height from which the drone was released into freefall. The freefall height was consistently set at 4.48 meters, while the drone payload weights were either 2.5lb (1.135kg) or 5lb (2.27kg). By maintaining a constant drop height and varying the payload weight, the initial potential energy of the drone differed between tests while ensuring that the testing equipment remained stationary, facilitating more reliable data collection. To establish a baseline for impact energy and injury level, the drone was first dropped without the spherical shell. Each test category included five trials, resulting in a total of 20 drop tests. The lower platform was precisely positioned beneath the upper platform bracket using a plumb bob to establish a vertical

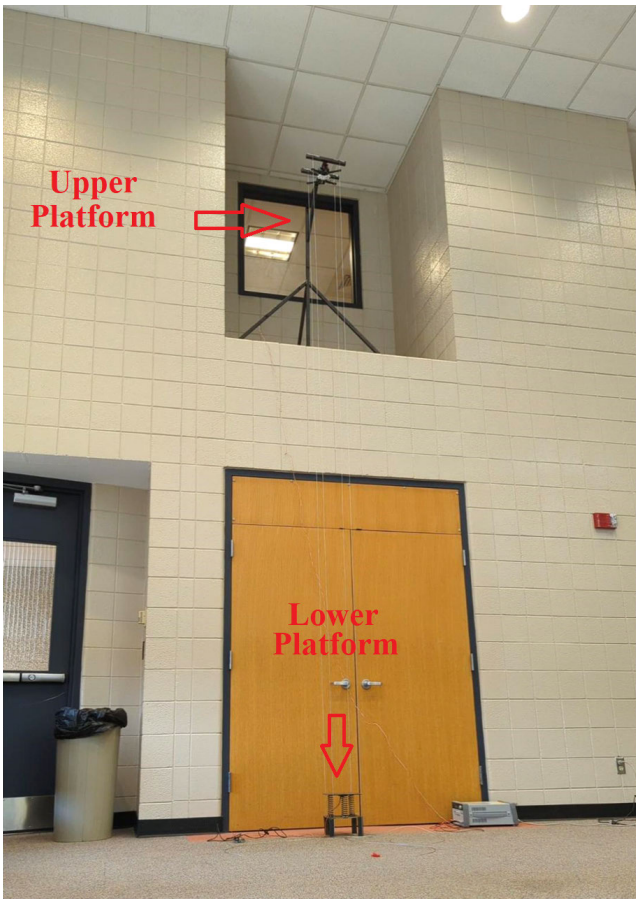

FIGURE 5. The drop test apparatus was utilized in Alumni Hall at SIU.

reference point relative to the bracket. During test trials, the lower platform exhibited significant shaking upon impact. To minimize this motion, weights were applied to stabilize the platform. As long as the frame remained intact, the impact energy absorbed by the test platform was not affected. The drone frame and shell components were only replaced in the event of structural failure.

The acceleration of the upper plate on the lower platform was measured to evaluate the AIS level during the drop test. The time interval chosen to record measurements was 0.05 seconds. Only the first peak of accelerometer data was evaluated, representing the initial impact the human head would experience. The impact time interval and the acceleration gathered on the Arduino program were recorded. The displacement of the drone before impact was measured with slow-motion footage, and the displacement and time between frames were used to measure the impact velocity.

D. HEAD INJURY CRITERION AND ABBREVIATED INJURY SCALE

To validate the physical experiments discussed above, we use a drag-inclusive energy model and map the results against the same AIS scale. Although these approaches differ in methodology, both ultimately aim to assess injury severity on the same AIS scale and we can include them in the same

AIS-based comparison plot like Fig. 8. The AIS is a widely used tool for classifying injury type based on the severity and type of injuries and was first developed in 1971 for defining injuries sustained from vehicle crashes [34]. It is maintained and revised by the Association for the Advancement of Automotive Medicine (AAAM). It is geared toward the survivability of an injury and is a global, anatomically based severity scoring system, which classifies each injury to a specific body region with a code from AIS1 to AIS6. Higher levels on the AIS scale indicate an increased risk of fatality. Energy, forces, or accelerations on human subjects or crash test dummies can be taken and converted to a certain level on the AIS. The Head Injury Criterion (HIC) is a tool used to evaluate the level of a head injury by predicting brain injuries or skull fractures to a certain severity. It is commonly used in automotive injury and is used by the US National Highway Traffic Safety Administration (NHTSA) to determine the crash-star rating for automobile safety. The relationship between impact head acceleration and the head injury criteria index is given as the following [35]:

$$\mathrm{HIC} = \left(\frac{1}{t_2 - t_1} \int_{t_1}^{t_2} a(t)\, dt \right)^{2.5} (t_2 - t_1) \tag{1}$$

where:

- a is the head acceleration measured in G-force, which is a measure of the force of gravity experienced by an object.

1G is equivalent to the gravity at the Earth's surface, while 2G is equivalent to twice the value of the gravity at Earth's surface. The values 1 and 2 are the selected starting and ending times measured in seconds, which can generate the largest HIC value as shown in Figure 6a [28].

In [36], HIC and AIS are correlated by the following expression:

$$\mathrm{AIS} = \begin{cases} C_{\mathrm{HIC}}^{\mathrm{AIS}}\, \mathrm{HIC}, & \text{if HIC} \leq 25, \\ C_{\mathrm{HIC}}^{\mathrm{AIS}}\, \mathrm{HIC} + \mathrm{Offset}_{\mathrm{HIC}}^{\mathrm{AIS}}, & \text{if HIC} > 25. \end{cases} \tag{2}$$

This expression comes from Figure 6b and is correlated only based on head-on impact tests using post-mortem experiments. It is simplified into the following expression:

$$\mathrm{AIS} = \begin{cases} \frac{1}{50}\, \mathrm{HIC} & \text{if HIC} \leq 25, \\ \frac{11}{3200}\, \mathrm{HIC} + 0.414 & \text{if HIC} > 25. \end{cases} \tag{3}$$

In [39], researchers investigate the correlation between impact force and injury severity level:

$$\mathrm{AIS} = \begin{cases} 3 & \text{if } 49.5\,\mathrm{J} < F \leq 99\,\mathrm{J}, \\ 4 & \text{if } F \geq 99\,\mathrm{J}. \end{cases} \tag{4}$$

This was done by conducting experiments on the thorax of anesthetized dogs, using a 1.75 kg impactor with a 5 cm circular face. The severity of the injuries was graded based on the AIS scale. The drop test experiments measure the total impact acceleration subjected to the top metal plate. It also measures the total displacement of the top metal plate and the time is also recorded. The slow-motion video allows a calculation of the velocity of the drone at the moment of impact. The velocity will be calculated by analyzing the successive frames in the video and measuring the displacement of the drone with the ruler attached to the lower platform. By using the known frame rate of the video, 240 frames per second, a calculation of the impact velocity can be made. To determine the impact energy of the drone at freefall, one must consider the forces of gravity and the drag forces that the drone is subjected to. The force of gravity can be expressed as the following:

$$F_g = m \cdot g \tag{5}$$

where:

- F_g is the gravitational force,
- m is the mass of the object,
- g is the acceleration due to gravity.

Where m is the mass of the drone and g is the gravitational constant. The drag forces can be represented by the following equation:

$$F_d = \frac{1}{2} c_d A \rho_A V_{\mathrm{rel}}^2 \tag{6}$$

where:

- F_d is the drag force,
- c_d is the drag coefficient,
- A is the reference area,
- ρ_A is the air density,
- V_{rel} is the relative velocity of the object.

When the drag force equals the force of gravity, the drone stops accelerating and has reached its terminal velocity. By solving for the velocity term, the equation becomes the following:

$$V_{\mathrm{rel}} = V_t = \sqrt{\frac{2mg}{c_d A \rho_A}} \tag{7}$$

where:

- V_t is the terminal velocity.

Assuming the initial velocity of the drone is 0, the impact velocity can then be expressed as the following [37]:

$$U = v_t \sqrt{1 - e^{(-\frac{2gh}{v_t^2})}} \tag{8}$$

where:

- U is the desired velocity,
- h is the height,
- e is the base of the natural logarithm.

Where u represents the impact velocity of the drone. The impact energy of the drone can then be expressed in the following formula:

$$E_{\mathrm{impact}} = \frac{1}{2} m u^2 \tag{9}$$

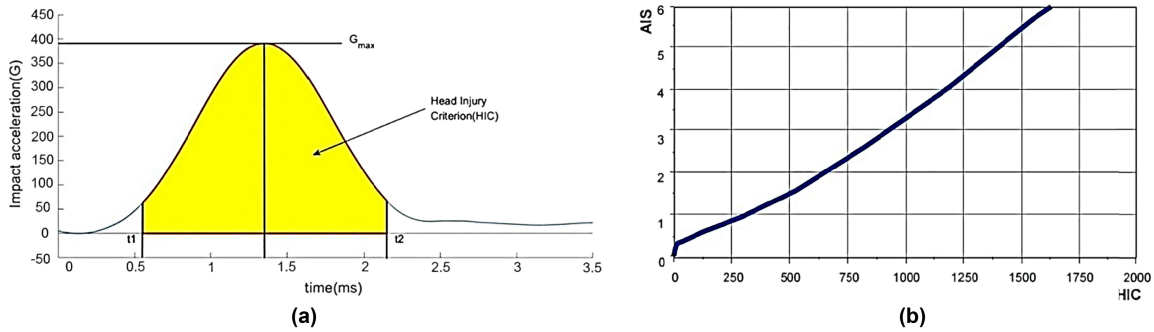

FIGURE 6. HIC and AIS graphs: (a) Illustrative example of an HIC calculation; (b) Correlation of HIC and AIS [12].

where:

- E_{impact} is the impact energy,
- m is the mass of the object,
- u is the velocity of the object.

E. FEA SIMULATIONS

A finite element analysis was conducted on the prototype structure using AutoDesk Inventor Pro to obtain preliminary data on the load intensity the structure could endure before experiencing plastic deformation. The material properties of the TPU-95A filament were incorporated into the simulation.

As depicted in Figure 7, one pentagon assembly was fully constrained, while another was subjected to a uniform pressure of 0.020 MPa, equivalent to a 98.1 N force applied over the outer surface area of the pentagon assembly. This force corresponds to the effect of a 10 kg load acting on top of the spherical cage. The analysis revealed that the maximum stress occurred at the joints of a shell connector. The resulting force of 231.6 MPa significantly exceeds the tensile strength of TPU-95A, which is 39 MPa, indicating a structural failure of the spherical shell connector.

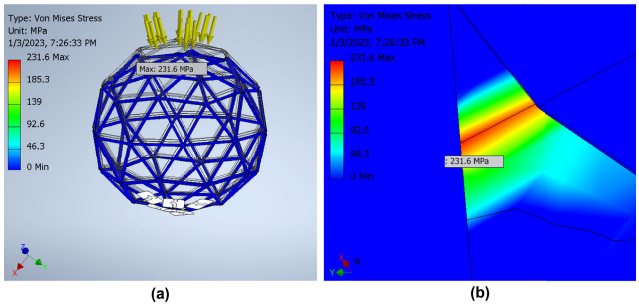

FIGURE 7. Structural analysis of spherical shell performed in AutoDesk Inventor Pro: (a) Complete view of the analyzed spherical shell; (b) The maximum stress concentrated at the connector joint.

III. RESULTS

The results presented in this section include preliminary findings and experimental drop tests, along with a comparison to simulation outcomes for validation and analysis.

A. PRELIMINARY RESULTS

In the simulation, Equations 8 and 9 are utilized to predict the impact energy and, consequently, the AIS level of a drone impact without a spherical shell across a range of heights and weights. The height varies from 3 m to 10 m, while the UAV mass ranges from 0.25 kg to 13 kg. The drag force coefficient is assumed to be 0.3, representing the lowest C_d value for a quadcopter [38]. The air density is considered at sea level, or 1.1225 kg/m^3. The cross-sectional area, A, for the QAV250 frame is 0.047 m^2.

The simulation results provide an estimate of the impact energy across varying drone weights and heights, as illustrated in Figure 8. The threshold for AIS3, corresponding to a minor skull fracture, is set at 95J, while AIS4, representing a major skull fracture, is set at 138 J, based on the experimental findings of Koh et al. [28].

As illustrated in the graph, in the absence of safety mechanisms to mitigate impact energy, drones weighing more than 3.5kg and dropped from a height of 4 meters are predicted to cause injuries exceeding AIS3 severity. Additionally, a drone with a mass of 1.25kg, when dropped from 10 meters, is not expected to result in an injury surpassing the AIS3 level. For a drop height of 5 meters, AIS3 injuries are predicted for drones weighing less than 2kg. These predictions align with the findings presented in [28].

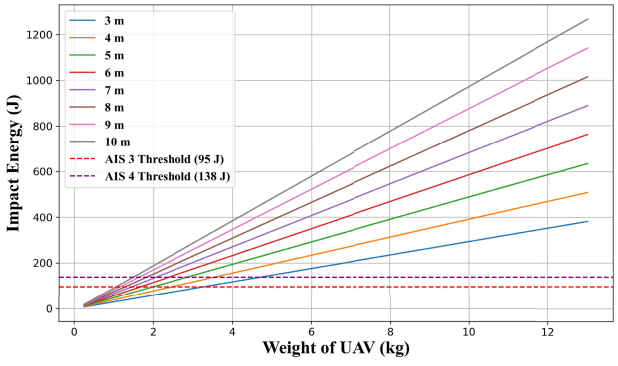

FIGURE 8. Estimated impact energy from free-fall analysis.

B. IMPACT ACCELERATIONS

Raw accelerometer data was taken from the GY-5201 accelerometer and logged in the Arduino Uno using a wired connection from the accelerometer to the Arduino and transmitted to a laptop to record the data. The serial clock and the serial pin were wired to the analog inputs on the Arduino Uno. The acceleration in the z-direction was considered the impact acceleration, as it corresponds to the vertical axis along which the impact occurred. Also, the total weight of the drone before drop tests was measured. This total weight includes the payload weight, the weight of the drone frame, the weight of the shell, and the weight of the metal piece used to connect the assembly to the electromagnet. The total weight of the shell after assembly was 0.68kg (1.5lb). The details of the total drone weight for both the 2.5-pound and 5-pound payloads, with and without the geodesic shell, are presented in Table 6.

TABLE 6. The detailed drone weight for different payload classes.

Items	ClassI Weight (2.5lb Payload)		ClassII Weight (5lb Payload)	
	No Shell	With Shell	No Shell	With Shell
Payload	2.5lb (1.134kg)	2.5lb (1.134kg)	5lb (2.268kg)	5lb (2.268kg)
Shell	0	1.5lb (0.68kg)	0	1.5lb (0.68kg)
Drone and Connectors	0.873lb (0.396kg)	0.873lb (0.396kg)	0.983lb (0.446kg)	0.983lb (0.446kg)
Total Weight	**3.373lb (1.53kg)**	**4.873lb (2.21kg)**	**5.983lb (2.71kg)**	**7.483lb (3.39kg)**

The first peak of the acceleration was analyzed as the immediate impact acceleration experienced on the lower test bed. These peaks are shown in Figure 9. The following peaks were not analyzed as they do not represent a realistic response to a dropped object on a human head. The peak time for drop tests ranged from 0.15-0.25 seconds for the 2.5lb weight class and 0.2-0.25 seconds for the 5lb weight class.

C. HIC AND AIS RESULTS

The definite integral of the accelerometer data was found by utilizing the trapezoidal rule, where the area under the curve of $f(x)$ over the interval [a, b] can be found using equation (10).

The equation for approximating an integral is:

$$\int_a^b f(x) \approx \frac{\Delta x}{2} \sum_{k=1}^{N} (f(x_{k-1}) + f(x_k)) \tag{10}$$

where:

- $\int_a^b f(x)$ is the integral of $f(x)$ from a to b,
- Δx is the width of each subinterval,
- $\sum_{k=1}^{N}$ is the summation from $k = 1$ to N,
- $f(x_{k-1})$ and $f(x_k)$ are the function values at the endpoints of each subinterval.

The definite integral and the time interval of the first peak are then used to find the HIC value of the drop test, using Equation 1. The HIC value is then used to find the AIS value using Equation 2. The AIS and HIC results of the drop tests are shown in Table 7 and Table 8.

TABLE 7. AIS and HIC results from 2.5lb payload weight class.

		Trial	HIC	AIS
2.5 lb	**No Shell**	1	451.9	1.97
		2	288.8	1.41
		3	308.5	1.47
		4	298.6	1.44
		5	418.4	1.85
		Average		**1.63**
	Shell	**Trial**	**HIC**	**AIS**
		1	500.1	2.13
		2	698.2	2.81
		3	458.4	1.99
		4	581.3	2.41
		5	702.1	2.83
		Average		**2.43**

TABLE 8. AIS and HIC results from 5lb payload weight class.

		Trial	HIC	AIS
5 lb	**No Shell**	1	1181.3	4.47
		2	1114.6	4.25
		3	1188.9	4.50
		4	1255.5	4.73
		5	1088.4	4.16
		Average		**4.42**
	Shell	**Trial**	**HIC**	**AIS**
		1	1328.3	4.98
		2	1053.3	4.03
		3	1473.3	5.22
		4	1164.9	4.42
		5	1368.9	5.12
		Average		**4.75**

As can be seen in the mentioned tables, the inclusion of the geodesic shell resulted in an increase in the AIS value for the drop test. This is due to where the geodesic shell failed upon impact, as well as the added weight of the shell. The overall structure of the shell remained intact during all the drop tests, and the points of failure occurred at the bottom connector where the carbon fiber rod secured the drone to the geodesic shell. Therefore, the energy was not transferred efficiently to the shell structure and did not significantly reduce the total impact acceleration.

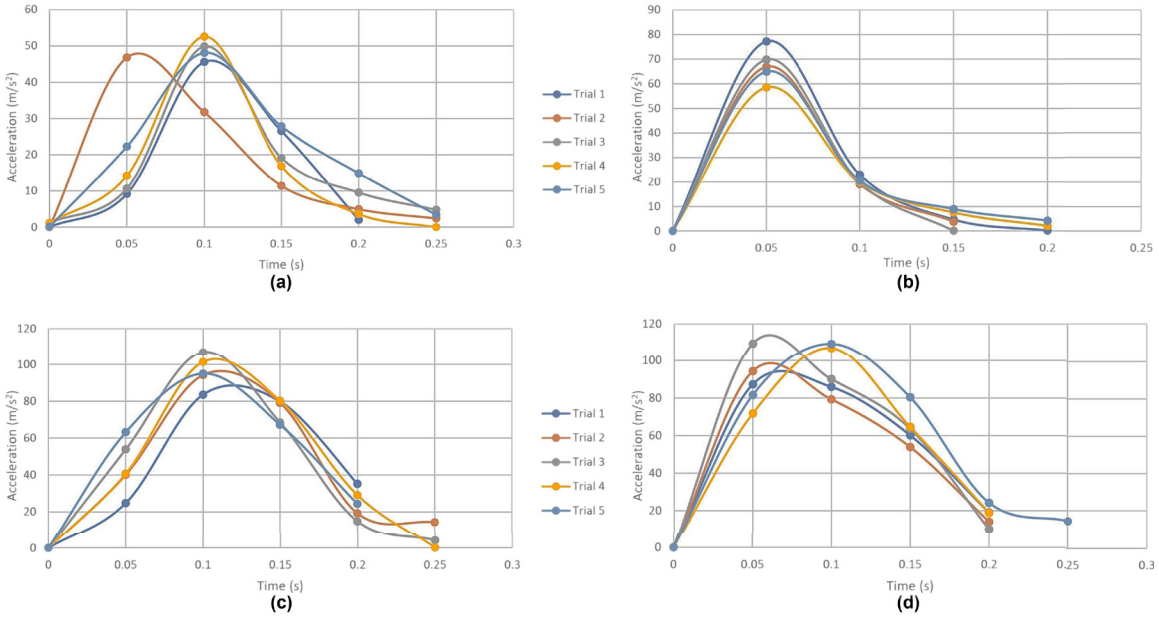

FIGURE 9. Impact acceleration graphs for all drop test classes and categories: (a) Acceleration-Time plot for 2.5 lb payload without shell; (b) Acceleration-Time plot for 2.5 lb payload with shell; (c) Acceleration-Time plot for 5 lb payload without shell; (d) Acceleration-Time plot for 5 lb payload with shell.

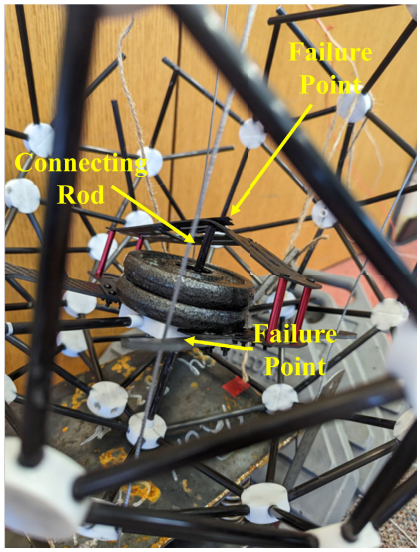

FIGURE 10. Shell failure during 2.5lb payload class.

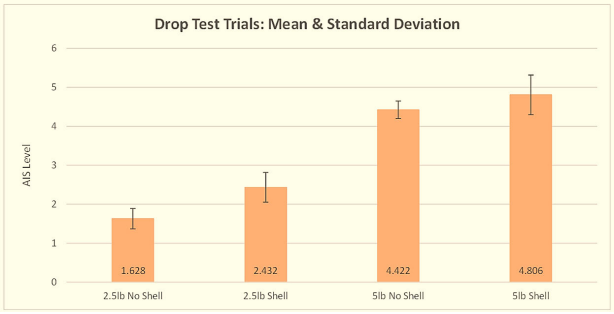

FIGURE 11. Drop test means and standard deviations.

TABLE 9. Impact energy thresholds and AIS levels.

Injury Level	AIS Code	Impact Energy Thresholds (J)	Probability of Fatality (%)
Minor	1	<19.8	0
Moderate	2	19.8–49.5	1–2
Serious	3	49.5–99	8–10
Severe-Critical	4–5	>99	5–50
Unsurvivable	6	>203.4	100

D. IMPACT ENERGY

Impact Energy was calculated by using the video captured for all drop tests. The displacement of the drone was measured using a ruler attached to the lower test bed. The time interval was calculated based on the number of frames used to measure displacement. The mass of the drone and impact velocity were then used in Equation 9 to calculate the total impact energy. The relation between impact energy and the AIS level was found in the work of [22]. Since AIS5 has the same probability of fatality as AIS4, the energy threshold of AIS5 is included with AIS4, as can be seen in Table 9.

The results of the impact energy calculations and AIS level threshold are found in Table 10. This table shows the energy threshold associated with a certain AIS value and is used to classify the impact energies found in the impact energy study with the associated AIS value. All values presented in this table were measured during the experimental tests.

The impact energy study yields less accurate results compared to the impact acceleration study, primarily due to the smaller number of data points available for energy-based calculations relative to velocity-based methods. The HIC is

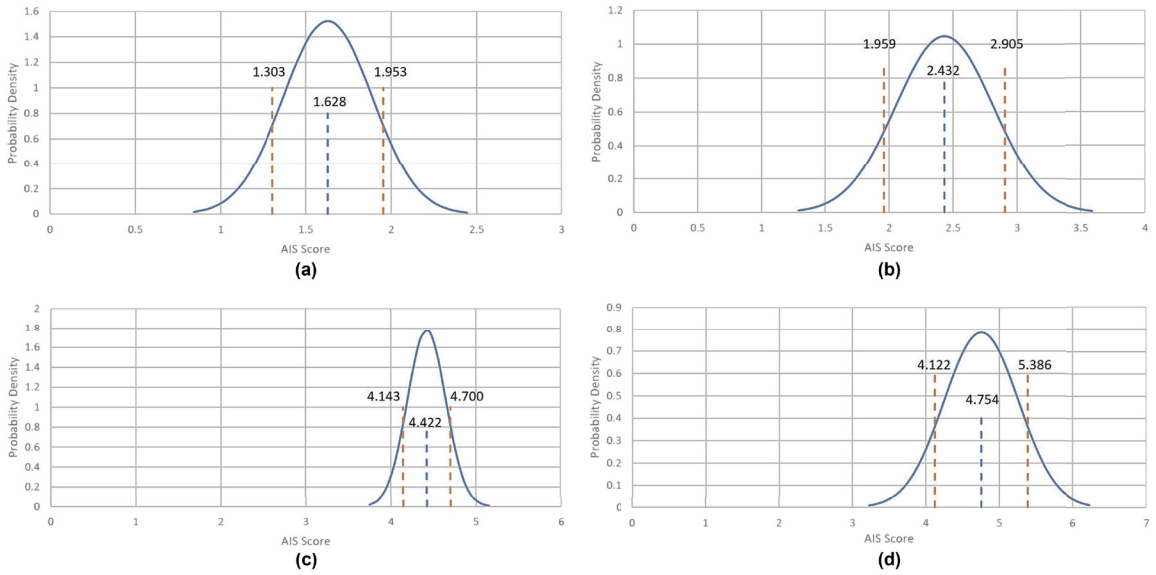

FIGURE 12. Confidence intervals across different payload classes: (a) 95% confidence interval for the 2.5 lb payload test without shell; (b) 95% confidence interval for the 2.5 lb payload test with shell; (c) 95% confidence interval for the 5 lb payload test without shell; (d) 95% confidence interval for the 5 lb payload test with shell.

TABLE 10. Impact energy results for 2.5lb and 5lb payloads.

Payload	Config	Parameters			
		Trials	Impact Velocity (m/s)	Impact Energy (J)	AIS Level Threshold
2.5 lb	No Shell	1	7.6	43.7	2
		2	7.4	41.9	2
		3	7.2	39.7	2
		4	7.2	39.7	2
		5	7.6	44.7	2
	Shell	1	7.2	57.5	3
		2	7.8	67.5	3
		3	7.5	62.4	3
		4	7.5	62.4	3
		5	7.8	67.5	3
5 lb	No Shell	1	8.4	95.6	3
		2	8.2	91.1	3
		3	8.4	95.6	3
		4	9.0	109.8	4-5
		5	8.4	95.6	3
	Shell	1	8.4	119.6	4-5
		2	8.5	122.5	4-5
		3	8.2	114.0	4-5
		4	9.1	140.4	4-5
		5	8.7	128.3	4-5

a widely adopted and extensively validated model for predicting head injury severity. In contrast, the model referenced in [25] is a more recent approach designed to estimate head injury levels using impact energy and regulatory thresholds established by national airspace authorities. While the HIC model relies on impact acceleration and is supported by decades of crash data from the National Highway Traffic Safety Administration (NHTSA), the model in [40] is based on a more limited dataset of accident cases. As a result, HIC is generally regarded as a more robust and reliable predictor of head injury risk.

E. SHELL FAILURE POINTS

During the drop tests with the shell, the point of failure occurred at the vertical connector that attached the drone to the geodesic shell. Instead of transferring the energy primarily into the shell, the vertical rod punctured through both the bottom drone frame and the bottom drone connector. Some energy was transferred due to friction losses when the bottom connector failed. In some cases, the vertical rod also punctured through the top drone frame. A typical result of the shell drop tests can be seen in Figure 10. The difference between the FEA prediction and experimental results can be justified by considering the actual failure location during impact. While finite-element analysis indicates a stress of 231 MPa in the TPU connector under a 10 kg load, far exceeding its reported tensile strength of 39 MPa, the connector does not fail in physical drop tests. This is because the shell fails at the interface between the drone frame and the connecting rod, which is structurally weaker than the connector itself. During impact, the force and energy are dissipated at this weaker interface, leading to its failure before the TPU connector reaches its critical stress threshold. As a result, the connector remains intact despite the high-stress predictions, highlighting the importance of failure path and load distribution in real-world conditions versus idealized simulations.

F. STATISTICAL ANALYSIS

Statistical analysis of the variance of the drop tests was performed to find a confidence interval that predicts how larger sample sizes of tests would behave. An alpha value of 0.05 was selected for a confidence interval of 95%. The standard deviation and the confidence intervals for the drop tests are found in Table 11. Additionally, the mean and standard deviations of the drop tests are shown in Figure11.

TABLE 11. Standard deviation and confidence intervals (95%) for all experiments.

Weight	Parameters			
	Config	Mean AIS Score	CI (95%)	Standard Deviation
2.5 lb	No Shell	1.628	±0.325	±0.262
	Shell	2.432	±0.473	±0.381
5 lb	No Shell	4.422	±0.279	±0.224
	Shell	4.754	±0.632	±0.509

As can be seen in Table 11, Figure 11, and Figure 12, the standard deviation and confidence interval of the drop tests with no shell are smaller than the standard deviation and confidence interval of the drop tests with the shell. It can be inferred that the drop tests with the shell fell in a less uniform way than the tests without the shell. This could be due to more energy being transferred to the shell in certain tests than others due to the friction losses at the bottom drone connector when failing, as well as the energy required for the bottom drone connector to fail. In contrast, in the drop tests without the shell, all of the energy is transferred to the lower drop test platform.

IV. CONCLUSION

A drop test apparatus was designed, built, and tested successfully. This drop test apparatus can simulate a drone falling with an initial velocity of 0 and striking a simulated human head to measure the impact acceleration and impact velocity. This allows a standard testing method to be applied to drone impacts. The design of the drop test apparatus proved to be a reliable and robust way to perform drop test experiments designed to measure the impact energy of a drone in free fall. The drone fell in a uniform way with minimal friction losses due to the steel guide wires. The drop test apparatus can be used to perform experiments with different payload weights, drop heights, and a variety of drone frames. The range of payload weights that can be performed is practically unlimited, with enough counterweight applied to the upper platform. The largest drone frame that can be tested with this apparatus is a 5'' rotor blade drone frame. However, the test apparatus can be modified to allow larger drone frames to be tested.

The findings of this study validate the successful development of a test bed apparatus designed to measure impact acceleration, impact force, and the corresponding HIC and AIS values of a falling drone used as a test specimen. Also, the addition of the geodesic sphere built with TPU and CFRP rods does not significantly reduce the AIS level of a direct drop on a simulated human head. The geodesic shell proved to be more robust than the drone connectors and did not absorb sufficient energy from the drop. This paper opens up a new area of research in testing the efficacy of drone shells in reducing head injury and measuring the amount of head injury sustained during a free fall of a UAV.

A. FUTURE WORKS

The designed drop test apparatus is a robust way to perform drop tests with UAV platforms and compare the impacts of different designs, such as designs with and without a geodesic shell, similar to what was done in this study as an example. Since this is a new area of research, previous research projects with drone shells can be extended to perform drop tests and determine the viability of the designed drone shell for reducing head injury. The test apparatus design also allows other safety methods that reduce impact energy to be tested. Since there are no commercial drone shells that protect the larger UAV platforms, attempts to commercialize a drone shell can use this method to establish a standard for head injury testing for their protective shell. Heavier payload classes and different material selections can also be researched using the designed shell and drop test apparatus.

ACKNOWLEDGMENT

The authors gratefully acknowledge the valuable guidance, discussions and feedback provided by Dr. James Mathias and Dr. Sabrina Nilufar of Southern Illinois University Carbondale.

REFERENCES

[1] W. Na, "A case analysis on Amazon delivery drones taking over traditional delivery method," *Int. J. Econ. Behav. Org.*, vol. 11, no. 1, pp. 1–6, Jan. 2023.

[2] A. Alizadeh, M. Farajijalal, Z. Rezvani, A. Toudeshki, and R. Ehsani, "Developing a data-driven model for predicting water stress in pistachio trees," in *Proc. Int. Congr. Agricult. Mechanization Energy Agricult.*, Switzerland, Oct. 2024, pp. 186–196.

[3] M. Narimani, A. Pourreza, A. Moghimi, M. B. Mesgaran, P. Farajpoor, and H. Jafarbiglu, "Drone-based multispectral imaging and deep learning for timely detection of branched broomrape in tomato farms," *Proc. SPIE*, vol. 13053, pp. 16–25, Feb. 2024.

[4] J. Abdulridha, A. Min, M. N. Rouse, S. Kianian, V. Isler, and C. Yang, "Evaluation of stem rust disease in wheat fields by drone hyperspectral imaging," *Sensors*, vol. 23, no. 8, p. 4154, Apr. 2023.

[5] F. Koerting, S. Asadzadeh, J. C. Hildebrand, E. Savinova, E. Kouzeli, K. Nikolakopoulos, D. Lindblom, N. Koellner, S. J. Buckley, M. Lehman, D. Schläpfer, and S. Micklethwaite, "VNIR-SWIR imaging spectroscopy for mining: Insights for hyperspectral drone applications," *Mining*, vol. 4, no. 4, pp. 1013–1057, Nov. 2024.

[6] H. Hildmann and E. Kovacs, "Review: Using unmanned aerial vehicles (UAVs) as mobile sensing platforms (MSPs) for disaster response, civil security and public safety," *Drones*, vol. 3, no. 3, p. 59, Jul. 2019.

[7] G. E. Jan, T. Lei, C.-C. Sun, Z.-Y. You, and C. Luo, "On the problems of drone formation and light shows," *IEEE Trans. Consum. Electron.*, vol. 70, no. 3, pp. 5259–5268, Aug. 2024.

[8] T. Askarzadeh, R. Bridgelall, and D. Tolliver, "Monitoring nodal transportation assets with uncrewed aerial vehicles: A comprehensive review," *Drones*, vol. 8, no. 6, p. 233, May 2024.

[9] S. Banker. (2022). *The Race for Last Mile Drones*. [Online]. Available: https://www.forbes.com/sites/stevebanker/2022/08/16/the-race-for-last-mile-drones/sh=41643e0c546f

[10] D. Zoldi. (Jun. 2022). *This Report Could Unleash the Potential of Commercial Drones*. [Online]. Available: https://www.forbes.com/sites/dawnzoldi/2022/03/14/this-report-could-unleash-the-potential-of-commercial-dronessh=6ec84edf3f21

[11] "Advisory and rulemaking committees UAS BVLOS ARC final report," U.S. Dept. Transp. (USDOT), Federal Aviation Admin. (FAA), Washington, DC, USA, 2022.

[12] "Treatment of the values of life and injury in economic analysis," U.S. Dept. Transp. (USDOT), Federal Aviation Admin. (FAA), Washington, DC, USA, 2022.

[13] M. Farajijalal, H. Eslamiat, V. Avineni, E. Hettel, and C. Lindsay, "Safety systems for emergency landing of civilian unmanned aerial vehicles (UAVs)—A comprehensive review," *Drones*, vol. 9, no. 2, p. 141, Feb. 2025.

[14] S. Malek, S. Salehkaleybar, and A. Amini, "Multi variable-layer neural networks for decoding linear codes," in *Proc. Iran Workshop Commun. Inf. Theory (IWCIT)*, Iran, May 2020, pp. 1–6.

[15] F. Khorsandi, G. De Moura Araujo, and F. Ferreira Lima dos Santos, "Artificial intelligence-driven all-terrain vehicle crash prediction and prevention system," *J. Agricult. Saf. Health*, vol. 30, no. 4, pp. 139–154, 2024.

[16] A. G. Waddell, "The use of artificial intelligence algorithms to improve the safety of unmanned aerial vehicles," Master's thesis, Dept. Elect. Comput. Eng., Major Elect. Eng., North Carolina Agricult. Tech. State Univ., Greensboro, NC, USA, 2021.

[17] D. Bianchi, A. Borri, S. Di Gennaro, and M. Preziuso, "UAV trajectory control with rule-based minimum-energy reference generation," in *Proc. Eur. Control Conf. (ECC)*, Jul. 2022, pp. 1497–1502.

[18] B. Mubdir and E. Prempain, "Energy-efficient trajectory optimization with nonlinear model predictive control for a quadrotor UAV," in *Proc. Eur. Control Conf. (ECC)*, Jun. 2024, pp. 3576–3581.

[19] B. Al-Madani, M. Svirskis, G. Narvydas, R. Maskeliūnas, and R. Damaševičius, "Design of fully automatic drone parachute system with temperature compensation mechanism for civilian and military applications," *J. Adv. Transp.*, vol. 2018, pp. 1–11, Nov. 2018.

[20] I. Indurkar, S. Mahajan, A. Soni, P. Chowdary, and A. Deepak, "Multipurpose low altitude UAV," Dept. Aerosp. Eng., Indian Institutes Technol. Madras, Chennai, India, Tech. Rep., 2021.

[21] L. Piancastelli, R. A. Bernabeo, M. Cremonini, S. Cassani, F. Calzini, and E. Pezzuti, "Optimized parachute recovery systems for remote piloted aerial systems," *J. Eng. Appl. Sci.*, vol. 13, no. 16, pp. 4590–4597, 2018.

[22] K. Edgerton, G. Throneberry, A. Takeshita, C. M. Hocut, F. Shu, and A. Abdelkefi, "Numerical and experimental comparative performance analysis of emerging spherical-caged drones," *Aerosp. Sci. Technol.*, vol. 95, Dec. 2019, Art. no. 105512.

[23] M. Dave, R. Patel, I. Joshi, and B. Goradiya, "Versatile multipurpose crashproof UAV: Machine learning and IoT approach," in *Proc. Int. Conf. Emerg. Technol. (INCET)*, Jun. 2020, pp. 1–7.

[24] S. Mizutani, Y. Okada, C. J. Salaan, T. Ishii, K. Ohno, and S. Tadokoro, "Proposal and experimental validation of a design strategy for a UAV with a passive rotating spherical shell," in *Proc. IEEE/RSJ Int. Conf. Intell. Robots Syst. (IROS)*, Sep. 2015, pp. 1271–1278.

[25] R. de Azambuja, H. Fouad, Y. Bouteiller, C. Sol, and G. Beltrame, "When being soft makes you tough: A collision-resilient quadcopter inspired by Arthropods' exoskeletons," in *Proc. Int. Conf. Robot. Autom. (ICRA)*, May 2022, pp. 7854–7860.

[26] J. Zha, X. Wu, R. Dimick, and M. W. Mueller, "Design and control of a collision-resilient aerial vehicle with an icosahedron tensegrity structure," *IEEE/ASME Trans. Mechatronics*, vol. 29, no. 5, pp. 3449–3460, Oct. 2024.

[27] P. D. Petris, H. Nguyen, M. Dharmadhikari, M. Kulkarni, N. Khedekar, F. Mascarich, and K. Alexis, "RMF-owl: A collision-tolerant flying robot for autonomous subterranean exploration," in *Proc. Int. Conf. Unmanned Aircr. Syst. (ICUAS)*, Jun. 2022, pp. 536–543.

[28] C. H. Koh, K. H. Low, L. Li, Y. Zhao, C. Deng, S. K. Tan, Y. Chen, B. C. Yeap, and X. Li, "Weight threshold estimation of falling UAVs (Unmanned aerial Vehicles) based on impact energy," *Transp. Res. C, Emerg. Technol.*, vol. 93, pp. 228–255, Aug. 2018.

[29] Y. Zhang, Y. Huang, K. Liang, K. Cao, Y. Wang, X. Liu, Y. Guo, and J. Wang, "High-precision modeling and collision simulation of small rotor UAV," *Aerosp. Sci. Technol.*, vol. 118, Nov. 2021, Art. no. 106977.

[30] A. Payne and S. Patel. (2001). *Injury Mechanism and Injury Criteria*. [Online]. Available: http://www.eurailsafe.net/subsites/operas/HTML/Section

[31] E. J. Hettel, "Spherical shell for low altitude UAV operations: An impact analysis," Ph.D. thesis, Dept. Mech., Aerosp. Mater. Eng., Southern Illinois Univ. Carbondale, Carbondale, IL, USA, Tech. Rep., 2023.

[32] *TPU-Raise3D: Reliable, Industrial Grade 3D Printer*. Accessed: Jul. 30, 2025. [Online]. Available: https://www.raise3d.com/filaments/tpu/

[33] S. Ciunel, A. Dută D. L. Popa, G. Popa-Mitroi, and V. Dumitru, "The behavior of the virtual human head-neck system during the main movements," *Appl. Mech. Mater.*, vol. 657, pp. 780–784, Oct. 2014.

[34] T. A. Gennarelli and E. Wodzin, "AIS 2005: A contemporary injury scale," *Injury*, vol. 37, no. 12, pp. 1083–1091, 2006, doi: 10.1016/j.injury.2006.07.009.

[35] D. Gao and C. W. Wampler, "Head injury criterion," *IEEE Robot. Autom. Mag.*, vol. 16, no. 4, pp. 71–74, Dec. 2009.

[36] P. Prasad and H. J. Mertz, "The position of the United States delegation to the ISO working group 6 on the use of HIC in the automotive environment," *SAE Trans.*, vol. 94, pp. 106–116, May 1985.

[37] G. R. Fowles and G. L. Cassiday, "Analytical mechanics," in *International Student Edition*, 7th ed., Pacific Grove, CA, USA: Brooks/Cole, 2005.

[38] P. A. Polivanov and A. A. Sidorenko, "Aerodynamic characteristics of a quadcopter with propellers," *AIP Conf. Proc.*, vol. 2351, May 2021, Art. no. 040053.

[39] L. M. Sturdivan, D. C. Viano, and H. R. Champion, "Analysis of injury criteria to assess chest and abdominal injury risks in blunt and ballistic impacts," *J. Trauma, Injury, Infection, Crit. Care*, vol. 56, no. 3, pp. 651–663, Mar. 2004.

[40] A. Shelley, "A model of human harm from a falling unmanned aircraft: Implications for UAS regulation," *Int. J. Aviation, Aeronaut., Aerosp.*, vol. 3, no. 3, pp. 1–23, 2016.

ERIC J. HETTEL received the B.S. degree in mechanical engineering and the M.S degree from Southern Illinois University, Carbondale, IL, USA, in 2021 and 2023, respectively. From 2019 to 2022, he was contracted to fabricate a test model of a hovercraft proposal for a local engineering firm. From 2021 to 2023, he was a Teaching Assistant for Dr. Hossein Eslamiat. He is currently working for P&G as a Process Engineer, primarily dealing with loss elimination and reliability engineering. His research interests include the fabrication of 3D printed prototype structures, safety controls for quadcopters, and the development of thermodynamic models for complex systems.

HOSSEIN ESLAMIAT received the B.S. degree in aerospace engineering from Sharif University of Technology, Tehran, Iran, in 2013, and the M.S. and Ph.D. degrees in mechanical and aerospace engineering from Syracuse University, Syracuse, NY, USA, in 2018 and 2020, respectively. He is currently an Assistant Professor of Mechanical Engineering with Southern Illinois University, Carbondale, IL, USA. His research interests include safety, control, dynamics, and estimation of unmanned aerial vehicles. He is a member of IEEE Technical Committee for Aerial Robotics and Unmanned Aerial Vehicles and a member of AIAA.

MOHAMMED ALEEMUDDIN received the B.S. degree in mechanical engineering from Jawaharlal Nehru Technological University Hyderabad, India, in 2023. He is currently pursuing the M.S. degree in mechanical engineering from Southern Illinois University, Carbondale, IL, USA. His research interests include safety systems of drones, autonomous flight systems, and metallic and non-metallic powders used in 3D printing processes in industry 4.0.

MOHSEN FARAJIJALAL received the B.S. and M.S. degrees in aerospace engineering from Sharif University of Technology, Tehran, Iran, in 2014 and 2017, respectively. He is currently a Research Assistant with the Mechanical Engineering Department, UC Merced, where his work focuses on smart agricultural systems, with a particular emphasis on agricultural robotics. His research interests include aerodynamics, CFD, remote sensing, agricultural, and aerial robotics.